INSTITUTE OF PHYSICS PUBLISHING JOURNAL OF PHYSICS: CONDENSED MATTER

J. Phys.: Condens. Matter **18** (2006) 4845–4851 doi:10.1088/0953-8984/18/20/009

Calculations for antiferrodistortive phase of $SrTiO_3$ perovskite: hybrid density functional study

E Heifets[1], E Kotomin[2] and V A Trepakov[3,4]

[1] Materials and Physics Simulation Center, Beckman Institute, California Institute of Technology, MS 139-74 Pasadena, CA 91125, USA
[2] European Commission, Joint Research Centre, Institute for Transuranium Elements, 76125 Karlsruhe, Germany
[3] Institute of Physics AS CR, Na Slovance 2, 182 21 Prague 8, Czech Republic
[4] A F Ioffe Physical-Technical Institute, 194 021 St-Petersburg, Russia

E-mail: heifets@wag.caltech.edu

Received 13 October 2005, in final form 10 April 2006
Published 2 May 2006
Online at stacks.iop.org/JPhysCM/18/4845

Abstract

The electronic and atomic structure of $SrTiO_3$ crystals below the antiferrodistortive phase transition observed at 105 K is calculated using the hybrid B3PW functional as implemented in the *ab initio* CRYSTAL-2003 computer code. Such a combination of non-local exchange and correlation permits the calculation for the first time of the TiO_6 octahedron rotational angle and the ratio c/a of tetragonal lattice constants in excellent agreement with experimental data. The level splitting of the bottom of the conduction band is found to be very small, <1 meV. The predicted phase-transition induced change of the optical gap from indirect to direct is confirmed by experimental photoconductivity data.

1. Introduction

Strontium titanate $SrTiO_3$ (hereafter STO) is a very particular and probably the best known model of ABO_3 perovskite-type oxides. Due to the wealth of unique properties and phenomena, many new ideas and original concepts of condensed matter and physics of phase transitions have been developed while investigating this unique material. At room temperature STO has the cubic (O_h^1) perovskite structure with five atoms per unit cell. At 105 K it undergoes an antiferrodistortive (AFD) $O_h^1 \rightarrow D_{4h}^{18}$ structural phase transition (PT) to a tetragonal phase with a doubled primitive unit cell of ten atoms [1–4]. The PT is caused by the antiphase tilting of the TiO_6 octahedra around one of the unit cell axes (hereafter the O_z axis), where the TiO_6 octahedra adjacent to one another along all O_x, O_y and O_z axes tilt in opposite directions. This PT is important not only as an excellent second-order phase transition model, but also because it leads to quantum paraelectric properties of STO observed at low temperatures.

Structural changes due to the AFD PT have been intensively studied in STO in a number of papers and are relatively well known. These changes could be characterized by the ratio

of the lattice parameters c/a (with the experimental value of 1.000 56 [5]) in the tetragonal phase and the TiO_6 octahedron rotation angle α (=2.1° [5]). The main features of the *electronic* (band) structure for a cubic phase of STO have been established long ago using semi-empirical methods (e.g., [6–9]). These results are in good agreement with a majority of relevant experiments (e.g. [10–14]). On the other hand, the interpretation of optical absorption and charge transport experiments performed around the AFD PT (e.g. [10, 12, 15] and references in [16]) needs more accurate theoretical studies. These calculations have to be performed at the *ab initio* level due to small changes in the atomic and electronic structure, as well as relative energy changes. Recently several DFT plane-wave calculations with ultrasoft pseudopotentials [17–20] were performed. These calculations considerably overestimate, by a factor of two to three, the rotation angle as well as the ratio c/a (e.g. 1.004 [17]). Simultaneously, these DFT calculations significantly underestimate the bandgap (typically, <2 eV, instead of experimental 3.3 eV) [17–21]. Surprisingly, an important question, how octahedral rotation affects the electronic bands and optical properties, has not been discussed so far, except for a single old paper [7]. These Koster–Slater tight-binding calculations included a simplified representation of O 2p states and neglected Ti e_g states which lie close to the Ti t_{2g} states. The 90 meV splitting of the lowest conduction bands at the Γ point into a lower double degenerate and upper non-degenerate levels was predicted.

In this paper, we report results of a precise study of the STO atomic and electronic structure changes due to the AFD PT based on calculations using the non-local Fock exchange in the framework of the *hybrid* DFT-HF approach. We demonstrate that such an approach fundamentally improves the quality of calculations and agreement with experiments, which permits reliable interpretation of optical properties of perovskites.

2. Computational details

The *ab initio* simulations were performed using CRYSTAL-2003 computer code [22, 23] with the local basis set of Gaussian-type basis functions. Here we applied the basis set recently developed specially for STO [21]. In these simulations we replaced nuclei and inner core electrons of Sr and Ti atoms with 'small-core' Hay–Wadt effective core potentials [24]. Outer core and valence electron density on Sr and Ti atoms as well as the entire electron density on O atoms were calculated explicitly using the Kohn–Sham equations. Crystalline orbitals were expanded in a basis set (BS) of atom-centred Gaussian-type functions (GTFs). The following BSs were constructed and optimized: 8-411(1d)G for O, 411(311d)G for Ti and 311(1d)G for Sr, where the numbers refer to the contraction level. Further details are available from [21].

Our experience shows that *hybrid* DFT–Hartree–Fock (HF) approach produces the lattice constant, elastic properties and bandgap of STO in the cubic phase in perfect agreement with experimental data. In present simulations, we employed the B3PW hybrid exchange–correlation functional [25] since it produced the best results in our previous studies. In B3PW the functional contribution of the exact non-local Fock exchange is 20%, and the remaining part is calculated with Becke's GGA functional [26]. The correlation part of the applied B3PW functional is described by the Perdew–Wang correlation functional [27].

The energy gain resulting from the AFD phase transition is extremely small. Therefore, we had to perform the computations with a very high precision. We set truncation criteria for bielectronic integrals to very tight values [22, 23]: all overlap thresholds for exchange integral series, overlap and penetration thresholds for Coulomb integrals were set to be 10^{-8}, and pseudo-overlap thresholds were set to 10^{-8} and 10^{-16}. We also had to use the finest of pre-defined grids (option XLGRID) for integration of exchange–correlation contributions in Kohn–Sham equations and the DFT total energy. Because high precision of the electronic

structure computations is needed, we also required high convergence (10^{-9} au) of the total energy in the solution of the Kohn–Sham equation.

STO in the AFD phase has a body-centred tetragonal lattice with the $I4/mcm$ symmetry group. We used the tetragonal primitive unit cell containing ten atoms or two cubic unit cells. The O_x and O_y axes in this unit cell are rotated by 45° with respect to those in the cubic unit cell. We followed the traditional expression for the AFD lattice constants through the parameters of a distorted cubic lattice [5]. In such notation periodicity along the O_z axis is characterized by the lattice constant $2c$, whereas the periodicity along the O_x and O_y axes is described by the lattice constant $a\sqrt{2}$. In the cubic lattice $a = c$. The ratio c/a is commonly used as a measure of the tetragonal distortion of perovskite crystals in the AFD phase. Tetragonal distortion in STO is very small with respect to the cubic fcc lattice. Therefore, the first Brillouin zone (BZ) nearly coincides with the BZ for the fcc lattice. In our calculations the integration over the BZ was done using the $8 \times 8 \times 8$ Monkhorst–Pack mesh [28].

In order to calculate atomic positions, we employed our own small code for geometry optimization. This code is an external optimization driver, which makes the inputs for CRYSTAL-2003 code from a template, reads the total energy from its output, and performs necessary computations for determining the next set of input parameters. The code uses final energy differences in order to calculate energy derivatives over optimization parameters. Then the conjugated gradient technique is used for performing the structure optimization. We optimized the STO structures for both phases. In the cubic phase, we fixed atoms in their high-symmetry positions and optimized the tetragonal unit cell, keeping the ratio of lattice constants fixed, in order to preserve the cubic phase. In the AFD phase, there are three independent parameters: two lattice constants along the O_z and O_x axes and the rotation angle of the of TiO_6 octahedra. (The lattice constant along the O_y axis is equal to the lattice constant along O_x axis due to crystal symmetry.)

In our previous simulations of perovskites [21] we used to shift up the energies of the conduction bands (*level shift*) in order to accelerate convergence of the density matrix and to ensure its stability. This is a common practice in such calculations. However, in the present simulations we found that the STO geometry optimization converges wrongly into a cubic structure, as soon as we try to apply this technique. We obtained the same result in our computations using the HF technique, which also overestimates the bandgap. This experience demonstrates that we have to apply a technique reproducing the crystal bandgap very accurately in order to be able to reproduce TiO_6 octahedron rotation and the corresponding AFD transition.

3. Results of computer simulations

For a cubic STO we obtained the lattice constant $a_0 = 3.912$ Å, which is only 0.35% larger than the experimental value of 3.898 Å. This gives a theoretical unit cell volume just 1% larger than the experimental one. The AFD phase transition leads to a small shrinking of the crystal due to a reduction of lattice constants along O_x and O_y axes. The theoretical unit cell volume in the AFD phase is only ∼1% larger than the experimental. The calculated ratio of the lattice constants $c/a = 1.0006$ is in perfect agreement with experiment [5]. Note that the previous computations employing the LDA functional [17] overestimated the c/a ratio (∼1.004). Our optimized octahedron rotation angle is equal to 1.95°, which again is in an excellent agreement with experiment [5]. Note that calculations performed with either LDA or GGA functionals usually strongly underestimate the bandgap of semiconductors and insulating crystals, including STO. All results of crystal structure optimization are assembled in table 1.

The calculated top of the valence band in a cubic STO is located at the *R*-point in the first BZ, which agrees with both theoretical results [6, 9] and two-photon absorption

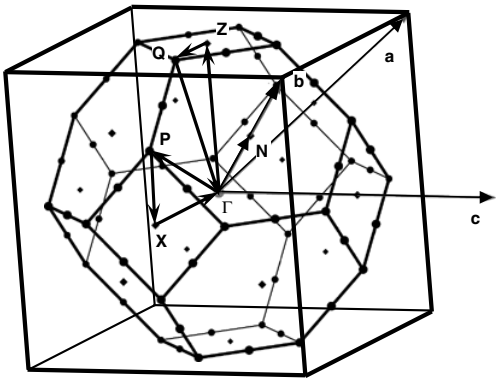

Figure 1. The first Brillouin zone of $SrTiO_3$ in the antiferrodistortive tetragonal phase; a, b and c are basis lattice vectors in the reciprocal space. The band structure in figure 2 is computed along the shown Γ–P–X–Γ–Z–Q–Γ–N path. Here the k-points are $\Gamma(0, 0, 0)$, $X(-0.5, 0.5, 0)$, $P(-0.25, 0.75, -0.25)$ and $N(0, 0.5, 0)$ [30], and additional labels were introduced for $Z(0.5, 0.5, -0.5)$ and $Q(0.25, 0.75, -0.5)$.

Table 1. Optimized structural parameters for $SrTiO_3$ in both cubic and AFD tetragonal phases. The numbers in brackets are experimental results [5]. The experimental data correspond to the temperatures around 110 K; theoretical calculations were done at 0 K, but could be corrected using the linear expansion coefficient $\alpha = 9.4 \times 10^{-6}$/K.

Cubic	Lattice constant, a_0 (Å)	3.912(3.898)
AFD	Lattice constant, a (Å)	3.910(3.894)
	Lattice constant, c (Å)	3.912(3.898)
	c/a	1.0006(1.0005)
	Octahedral rotation angle, α	1.95°(2.1°)
	Energy gain, ΔE (eV)	0.00021

experiments [14]. The band structure for the cubic STO calculated using the same computational conditions was published earlier [21]. There are nearly flat regions of the upper valence band between the R and M points. The lowest conduction band bottom lies at the Γ point with the flat region towards the X point, which is consistent with previous band structure calculations [6–9]. The present computations give a slight overestimate (3.70 eV) for the *indirect* R–Γ bandgap (experimental value 3.22–3.25 eV [11, 13, 28], 3.35 eV [14]) and 4.03 eV for the direct Γ–Γ gap (3.75 eV in experiment [28] and 3.79 eV in [14]). The AFD phase transition causes doubling of the crystal primitive unit cell and corresponding folding of the first BZ. This leads to merging of both the R and Γ points of the cubic structure into the Γ point of the BZ of the AFD tetragonal phase (figure 1). Similarly, both the M and X points of a cubic phase merge into the X and Z points after the phase transition. As a result, optical transitions between energy states corresponding to the flat band regions turn out to be *direct*.

Results of our electronic structure calculations are summarized in figure 2 and table 2. Figure 2 illustrates the behaviour described above for the bands along the Γ–Z and Γ–X directions. The bandgap increases by 12 meV in the AFD phase as compared to the cubic phase. The double-degenerated states at the conduction band bottom at the Γ point lie above non-degenerated state only by 0.8 meV. Such a level sequence is opposite to that predicted in [22] and much smaller in magnitude. The difference might be caused by neglecting in [22] the mixing of e_g states with t_{2g} at the conduction band bottom.

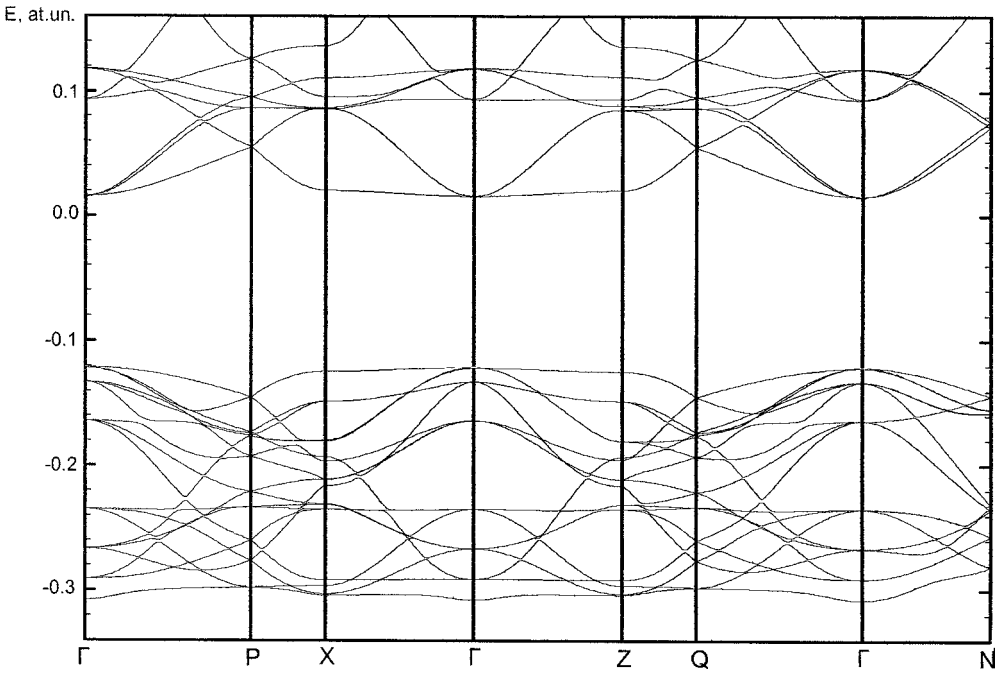

Figure 2. Band structure of $SrTiO_3$ in the antiferrodistortive tetragonal phase.

4. Discussion and conclusions

We calculated in this paper the atomic and electronic structure of STO in the AFD phase. The characteristic parameters of the crystalline structure obtained are very close to experimental values. This is a result of the combination in the hybrid functional of non-local (Fock) exchange and correlation effects. The calculated changes in the band structure and, especially, predicted transformation of the lowest in energy $R \rightarrow \Gamma$ indirect transition in the cubic phase into the direct $\Gamma \rightarrow \Gamma$ transition in the AFD phase could produce visible changes in an experimental shape of fundamental absorption edge [12] and other electronic structure-related properties (e.g. electronic transport [9] and piezo-resistance [11]), conductivity and photoconductivity. For example, just recently an unusual temperature behaviour of the maximum of the photoconductivity spectrum was experimentally found in STO in the region of the AFD phase transition [15]. Conventionally, the photoconductivity increases as the excitation energy approaches the band edge, rises in the region of the indirect optical transition onset and goes over the maximum in the region of the most intensive band-edge transitions. Lastly, it decreases at higher energies due to increase of the photo-electron–hole recombination rate, thus approaching the surface recombination photoconductivity limit [31]. The position of the maximum of the photoconductivity excitation spectrum shifts *monotonically* to higher energies upon cooling due to increase of the optical bandgap. This conventional behaviour was indeed observed [15] in STO *above* the AFD PT in the cubic phase. However, in the AFD region, the maximum position of excitation energy spectra for the photoconductivity reveals unusual non-monotonic temperature behaviour. This peculiarity arises because the lowest in energy, indirect phonon-assisted $R \rightarrow \Gamma$ optical transition is weak in a cubic phase (above the phase transition) and therefore practically does not affect the photoconductivity spectra maximum. However, our theoretical analysis shows that in the AFD phase this transforms into

Table 2. The calculated energy gaps between different k-points of the BZ of the cubic and AFD tetragonal phases of STO. Values in brackets are experimental data [29]; those marked (*) are two-photon absorption data [14].

Cubic phase		Antiferrodistortive tetragonal phase	
Optical gap	Transition energy (eV)	Optical gap	Transition energy (eV)
$\Gamma \rightarrow \Gamma$	4.0282	$\Gamma \rightarrow \Gamma$	4.0304
	4.0284		4.0312
	(3.75, 3.79*)		4.0314
			4.0322
$\Gamma \rightarrow X$	4.1623	$\Gamma \rightarrow Z$	4.1635
			4.1645
		$\Gamma \rightarrow X$	4.1620
			4.1630
$R \rightarrow \Gamma$	3.7048	$\Gamma \rightarrow \Gamma$	3.7168
	3.7050		3.7176
	(3.25, 3.35*)		3.7358
			3.7366
$R \rightarrow X$	3.8389	$\Gamma \rightarrow Z$	3.9428
		$\Gamma \rightarrow X$	3.9383
$M \rightarrow \Gamma$	3.8008	$Z \rightarrow \Gamma$	3.8097
	3.8011		3.8106
	3.55*		
		$X \rightarrow \Gamma$	3.8067
			3.8075
$M \rightarrow X$	3.9349	$Z \rightarrow Z$	3.9428
		$X \rightarrow Z$	3.9398
		$X \rightarrow X$	3.9383
		$Z \rightarrow X$	3.9413

the direct $\Gamma \rightarrow \Gamma$ transition whose probability is known to be much larger [31]. For this reason, this transition begins to play an important role in the shape of the photoconductivity spectra. As a result, the maximum position of the photoconductivity spectrum shifts to the lower energy side, which leads to the experimentally observed non-monotonic temperature behaviour of the maximum of the photoconductivity spectrum.

Acknowledgments

This work was supported by project AV0Z 10100522 of the AS CR and RFBR 03-02-17589 (VT). The authors are indebted to R Evarestov, F Illas, T Gouder, G Lander and R Konings for numerous discussions.

References

[1] Müller K A 1958 *Helv. Phys. Acta* **31** 173
[2] Fleury P A, Scott J F and Worlock J M 1968 *Phys. Rev. Lett.* **21** 16
[3] Courtens E 1972 *Phys. Rev. Lett.* **29** 1389
[4] Cowley E A 1996 *Phil. Trans. R. Soc.* A **354** 2799
[5] Lytle F W 1964 *J. Appl. Phys.* **35** 2212
[6] Kahn A H and Layendeccker J 1964 *Phys. Rev.* **135** A1321

[7] Mattheiss L F 1972 *Phys. Rev.* B **6** 4718
[8] Wolfram T, Krant E A and Morin F J 1973 *Phys. Rev.* B **7** 1677
[9] Zook J D and Casselman T N 1973 *Surf. Sci.* **37** 244
[10] Frederikse H P R, Thurber W R and Hosler W R 1964 *Phys. Rev.* **134** A442
[11] Cardona M 1965 *Phys. Rev.* **140** 651
[12] Tufte O N and Stelzer E L 1966 *Phys. Rev.* **141** 675
[13] Capizzi M and Frova A 1970 *Phys. Rev. Lett.* **27** 1298
Capizzi M and Frova A 1972 *Solid State Commun.* **10** 1165
[14] Shablaev S I, Danishevskii A M and Subashiev V K 1984 *Zh. Eksp. Teor. Fiz.* **86** 2158
[15] Katsu H, Tanaka H and Kawai T 2000 *Japan. J. Appl. Phys.* **39** 2657
[16] Galinetto P, Rsella F, Samoggia G, Trepakov V, Kotomin E, Heifets E, Markovin P and Jastrabik L 2006 *Ferroelectrics* at press
[17] Sai N and Vanderbilt D 2000 *Phys. Rev.* B **62** 13942
[18] Buban P, Iddir H and Ogut S 2004 *Phys. Rev.* B **69** 180102
[19] Astala R and Bristowe P D 2001 *Comput. Mater. Sci.* **22** 81
Astala R and Bristowe P D 2001 *Modelling Simul. Mater. Sci. Eng.* **9** 415
[20] Uchida K, Tsuneyuki S and Schimizu T 2003 *Phys. Rev.* B **68** 174107
[21] Piskunov S, Heifets E, Eglitis R I and Borstel G 2004 *Comput. Mater. Sci.* **29** 165
Piskunov S, Heifets E, Kotomin E, Maier J, Eglitis R and Borstel G 2005 *Surf. Sci.* **575** 75
[22] Saunders R, Dovesi R, Roetti C, Orlando R, Zicovich-Wilson C M, Harrison N M, Doll K, Civalleri B, Bush I J, D'Arco Ph and Llunell M 2003 *CRYSTAL2003 User's Manual*
[23] http://www.chimifm.unito.it/teorica/crystal/crystal.html
[24] Hay P J and Wadt W R 1984 *J. Chem. Phys.* **82** 299
[25] Becke A D 1993 *J. Chem. Phys.* **98** 5648
[26] Becke A D 1988 *Phys. Rev.* A **38** 3098
[27] Perdew J P and Wang Y 1986 *Phys. Rev.* B **33** 8800
Perdew J P and Wang Y 1989 *Phys. Rev.* B **40** 3390
Perdew J P and Wang Y 1992 *Phys. Rev.* B **45** 13244
[28] Monkhorst H J and Pack J D 1976 *Phys. Rev.* B **13** 5188
[29] van Benthem K, Elsaesser C and French R H 2001 *J. Appl. Phys.* **90** 6156
[30] http://www.cryst.ehu.es/cryst/get_kvec.html
[31] Bube R 1960 *Photoconductivity of Solids* (New York: Wiley)